JOURNAL OF COMPUTATIONAL PHYSICS 110, 310–319 (1994)

Electromagnetics via the Taylor–Galerkin Finite Element Method on Unstructured Grids

JOHN J. AMBROSIANO AND SCOTT T. BRANDON

Lawrence Livermore National Laboratory, Livermore, California

RAINALD LÖHNER

CMEE School of Engineering and Applied Science, George Washington University, Washington, DC

AND

C. RICHARD DEVORE

Laboratory for Computational Physics and Fluid Dynamics, Naval Research Laboratory, Washington, DC

Received May 8, 1991; revised November 19, 1992

Traditional techniques for computing electromagnetic solutions in the time domain rely on finite differences. These so-called FDTD (finite-difference time-domain) methods are usually defined only on regular lattices of points and can be too restrictive for geometrically demanding problems. Great geometric flexibility can be achieved by abandoning the regular latticework of sample points and adopting an unstructured grid. An unstructured grid allows one to place the grid points anywhere one chooses, so that curved boundaries can be fit with ease and local regions in which the field gradients are steep can be selectively resolved with a fine mesh. In this paper we present a technique for solving Maxwell's equations on an unstructured grid based on the Taylor–Galerkin finite-element method. We present several numerical examples which reveal the fundamental accuracy and adaptability of the method. Although our examples are in two dimensions, the techniques and results generalize readily to 3D.

1. INTRODUCTION

Traditional techniques for computing electromagnetic solutions in the time domain rely on finite differences. These so called FDTD (finite-difference time-domain) methods [1–3] are applicable to a broad range of problems and are both reliable and accurate. However, the regular lattices of points on which the finite-difference operators are defined can be too restrictive for geometrically demanding problems. In particular, problems in which there is scattering from an object of complicated shape, or problems requiring extreme local refinement of zones, are not well suited to a regular finite difference grid. Geometric flexibility can be achieved by abandoning the regular latticework of sample points. Several useful approaches have evolved from the strategy of deforming the mesh and using curvilinear coordinates with finite differences [4]. Another strategy is to adopt unstructured grids and employ finite-volume or finite-element methods [5–11]. Traditionally, finite element methods have been applied to electromagnetics in the frequency domain, although the importance of applying these methods in the time domain has recently been recognized [8, 9]. An unstructured grid connects a given point to an arbitrary number of other grid points. Typically the points are connected to form triangles in 2D or tetrahedra in 3D. An unstructured grid provides the greatest flexibility by allowing one to place the grid points anywhere one chooses, so that curved boundaries can be fit with ease. One can also refine local areas of interest, either *ab initio* or dynamically, without unduly affecting the resolution in other parts of the problem domain.

In this paper we present a technique for the efficient solution of Maxwell's equations on an unstructured grid. An idea that we wish to stress, and whose importance should become clear as our presentation unfolds, is that it is the combination of the numerical technologies of unstructured-grid generation and refinement on the one hand, and of the basic Taylor–Galerkin procedure and its enhancements on the other, that make our approach to computational electromagnetics so powerful. Thus, we begin by describing in Section 2 the methods used to generate and refine the unstructured meshes for our electromagnetic calculations.

0021-9991/94 $6.00

In Section 3, we follow with an exposition of the Taylor–Galerkin finite-element method as applied to electromagnetics. We discuss our results and present our conclusions in Section 4.

2. UNSTRUCTURED-GRID GENERATION AND REFINEMENT

The generation of an unstructured grid appropriate to a given problem (in hydrodynamics, aerodynamics, or electromagnetics) is a task that, while computationally intensive, fortunately can be largely automated. The grid generator can concentrate the points where they are needed and disperse them where they are not. The problem of smoothly interfacing regions of very different grid resolution is vastly simplified. Because the recent use of unstructured grids allows the modelling of problems with complex geometries and varying length scales, we feel that automatic unstructured grid generation is an integral part of the present contribution. Therefore, we will describe the generation and adaptation of unstructured grids in detail here, rather than referring the reader to other publications.

To create an unstructured grid for the problem at hand, one must first specify a set of curves in 2D (or a set of surfaces in 3D) that define the boundaries of the computational domain. In addition, it may be advantageous to associate with certain subregions of the domain some particular gridding preferences: the zone size, the zone stretching ratio (ratio of the longest side to the shortest side), and the zone orientation. Beyond these basic requirements, the task of grid construction should be essentially automatic.

We use an automated grid-generation method known as the advancing-front technique [12, 13]. Figure 1 illustrates the basic idea. A boundary curve in 2D (surface in 3D) is specified via a set of points joined by straight segments or cubic splines. Gridding preferences are specified at each point on a coarse background mesh. This background mesh is itself an unstructured mesh of triangles (tetrahedra).

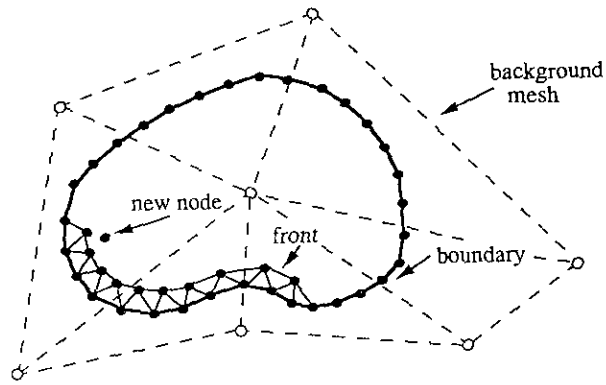

FIG. 1. A schematic illustration of the advancing front method. A background mesh provides the generator with information about zone preferences at different places in the domain. The boundary faces constitute the initial front that then moves into the computational domain as elements are added to the grid.

Once the boundary and the background mesh are described to the generator, the creation of the mesh proceeds automatically. Mesh creation via the advancing front method involves several ingenious steps and some special data structures [12]. Interpolating from the background mesh to points on the boundary curve (surface), the generator first discretizes the boundary into a contiguous set of line segments (triangular faces) which is called the front. Starting in the vicinity of the shortest segment (smallest face), a point is added to form a triangular

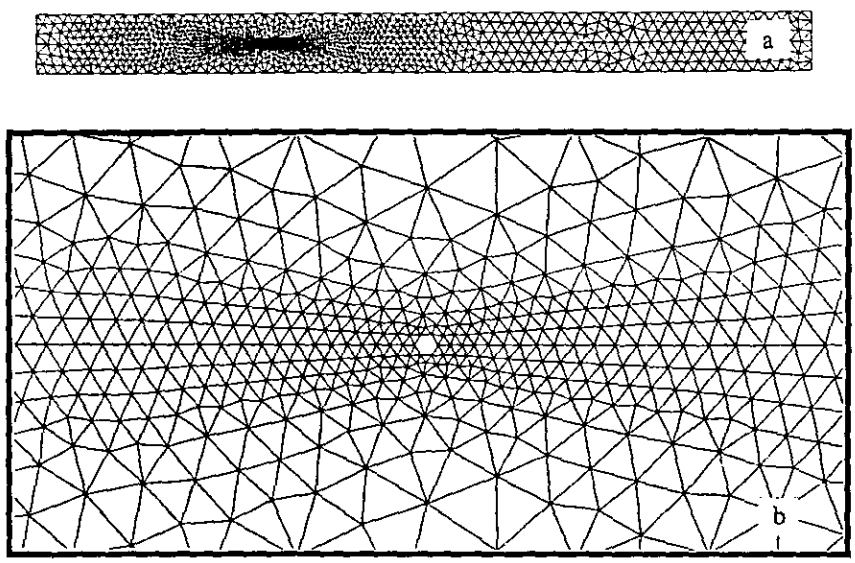

FIG. 2. An unstructured mesh for a geometrically stiff problem: (a) A small wire occupies a portion of a much larger domain. (b) A closeup of the grid reveals the grid immediately surrounding the wire.

(tetrahedral) element. The optimal location for the new point is chosen by again interpolating the desired element characteristics from the nodes of the background mesh. The segment (or face) behind the new element is then deleted from the segment (face) list and the new segments (or faces) are added to update the definition of the front. This procedure continues until the entire region is filled. In situations where choosing the optimal point would create an element that collides with another portion of the front (i.e., the optimal point lies behind rather than ahead of the front), the best neighboring point on the front is chosen. Finally, the initially generated mesh can be relaxed by applying tension to the nodes or refined by subdivision, or both.

As an example of the advantages of using an unstructured grid for a problem requiring extreme local refinement, we present Fig. 2. The grid here is rather long and has a very fine wire embedded within it. In the computation, to be described in Section 3, the upper and lower boundaries were periodic, so that we actually are simulating an array of wires. The wire is located within the densely zoned region of Fig. 2a and its radius is only 1/150th of the width of the region. A closeup of the zones near the wire is shown in Fig. 2b. The unstructured grid allows us to use these very fine zones near the wire and smoothly match them to coarser zones in the remainder of the domain. The total number of elements in this grid is 3614. If we were forced to solve this problem using a uniform grid with one zone resolving the wire, some 540,000 elements would be required.

The advancing-front grid generator adds new points to the mesh being constructed according to the gridding preferences specified for the background mesh. Of course, the optimal choices for these preferences may depend sensitively upon the solution to be obtained, and thus they are the subject of insight and informed guesswork in the construction of the initial mesh. Two methods are available for refining such a preliminary mesh. The first is a dynamical technique known as *H* refinement [15], and its principle of operation is quite simple. One develops a criterion, usually based on the magnitude of the first or second spatial derivatives of the field variables for establishing local bounds on the element sizes required to resolve the instantaneous structure of the fields. If an element becomes larger than the requisite upper bound, it is subdivided. In 2D, one triangular element is replaced by four; in 3D, one tetrahedral element is replaced by eight. The data structure linking the nodes, faces, and elements are all updated, the new objects being added at the ends of the appropriate lists, and the calculation proceeds.

A second method for refining a preliminary mesh is adaptive remeshing [16, 17]. This technique is particularly well suited for problems in which high accuracy is required and for which the cost of obtaining a sequence of progressively better solutions is not prohibitive. As in the *H*-refinement approach, one prescribes a criterion for establishing local bounds on the element sizes and for selecting stretching factors and orientations as well. Rather than instananeously refining the mesh, however, this information is accumulated throughout the calculation and written out at its end. Then the preliminary mesh and the gridding preferences derived from the accumulated information are used to define the background mesh for a second pass through the grid generator. The initial mesh thereby is adaptively refined to reflect the local properties of the solution, and this new mesh can be used to obtain a more accurate solution. The procedure may be repeated as many times as is needed.

To illustrate the process of adaptive remeshing, we show in Fig. 3 two griddings of a cylindrical scattering problem. The grid in Fig. 3a is the initial grid, constructed from a simple background mesh specifying a uniform element size and some stretching of the elements near the outer boundary along the azimuthal coordinate, i.e., transverse to the direction of propagation of the outgoing scattered waves. The incident wave is a monochromatic plane wave propagating to the right, with a wavelength equal to 1/10th the circumference of the cylinder. After evolving the solution for several wave periods, we used an error indicator based on the spatial derivatives to set the new element sizes, and element stretching again was allowed near the outer boundary in the direction transverse to the local direcion of propagation. In this adaptive remeshing, the minimum element size

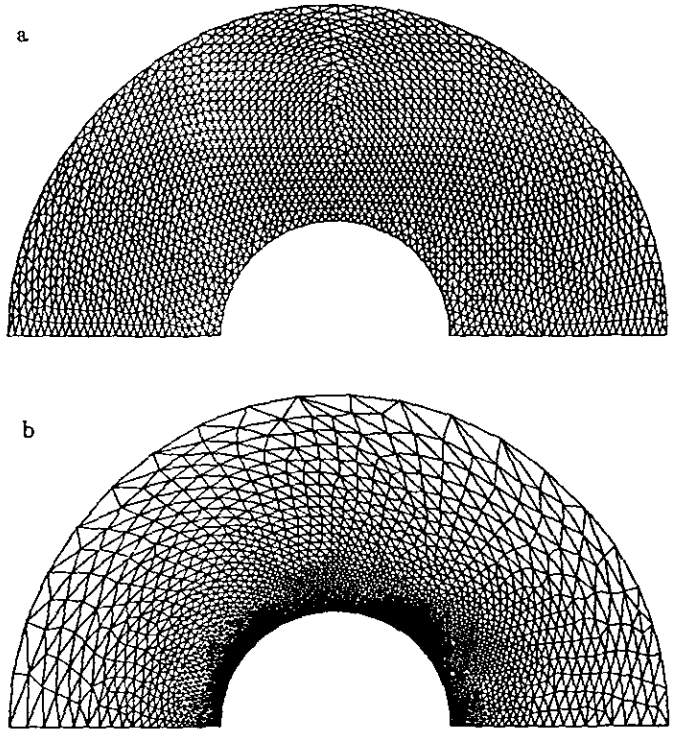

FIG. 3. An example of adaptive remeshing for the scattering of a plane wave from a circular cylinder. Information from a preliminary steady-state calculation on the *ab initio* mesh (a) is used to generate an optimized new grid (b) for a more accurate calculation.

was reduced near the cylinder for improved accuracy in the computed fields there and increased near the outer boundary to reduce the number of zones where such high resolution is unnecessary. We show the mesh which resulted from the subsequent pass through the grid generator in Fig. 3b. The number of points in the grid increased by roughly 25% during the rezoning, from 1977 to 2589. More important, however, is the redistribution and resizing of the elements to provide an optimal mesh for accurately solving the problem. The success of this strategy will become evident later in Section 3, when we present the resulting solution.

3. THE TAYLOR-GALERKIN METHOD APPLIED TO ELECTROMAGNETICS

In the time domain, electromagnetics is essentially a hyperbolic problem. Until recently, it was believed that finite elements were not a good match to hyperbolic systems of partial differential equations (PDEs). However, Taylor–Galerkin methods [18, 19] have proven very successful in such applications—specifically in computational fluid dynamics. Donea [18], who is largely responsible for the introduction of these methods, has analyzed Taylor–Galerkin schemes for linear advection and has found that they have good stability and low phase error.

Donea found that attending to the temporal truncation error before spatial discretization consistently produced better results than had previously been achieved with Galerkin methods. Our expectation was that these qualities would carry over to electromagnetic applications, and we have thus far not been disappointed.

The idea behind the Taylor–Galerkin formulation is very simple. One first specifies a temporal truncation error by expanding the unknowns in a Taylor series. The PDE is then used to replace partial derivatives in time with partial derivatives in space. Finally a Galerkin finite-element approximation is applied to the spatial derivative operators. To illustrate, consider the simple linear hyperbolic system in 1D,

$$\frac{\partial u}{\partial t} = -\frac{\partial f(u)}{\partial x} = -c\frac{\partial u}{\partial x}, \tag{1}$$

where $c \equiv \partial f(u)/\partial u$ is the characteristic speed which is independent of u for linear problems. We expand the unknown at time level $n+1$ about the value at time level n,

$$u^{n+1} = u^n + \Delta t\left(\frac{\partial u}{\partial t}\right)^n + \frac{1}{2}\Delta t^2\left(\frac{\partial^2 u}{\partial t^2}\right)^n + O(\Delta t^3). \tag{2}$$

Substituting expressions for the time derivatives from (1) into (2), we obtain

$$u^{n+1} = u^n - c\,\Delta t\left(\frac{\partial u}{\partial x}\right)^n + \frac{1}{2}c^2\,\Delta t^2\left(\frac{\partial^2 u}{\partial x^2}\right)^n. \tag{3}$$

This procedure is similar to one for deriving the Lax–Wendroff scheme [20], and in fact, if one replaces the derivatives with centered finite differences, Lax–Wendroff is obtained. Instead we apply the Galerkin approximation. We expand u^n as

$$u^n(x) = \sum_i u_i^n N_i(x), \tag{4}$$

where $N_i(x)$ is the nodal linear basis or shape function and u_i is the value of u at node i. On substituting (4) into (3) and taking the inner product with another shape function $N_j(x)$, we obtain

$$\sum_i \langle N_j | N_i \rangle \,\delta u_i = -c\,\Delta t \sum_i \left\langle N_j \middle| \frac{\partial N_i}{\partial x} \right\rangle u_i^n - \frac{1}{2}c^2\,\Delta t^2 \sum_i \left\langle \frac{\partial N_j}{\partial x} \middle| \frac{\partial N_i}{\partial x} \right\rangle u_i^n. \tag{5}$$

Here $\langle F | G \rangle \equiv \int F(x)\,G(x)\,dx$ is the inner product and $\delta u \equiv u^{n+1} - u^n$. The left-hand side involves the operation of the consistent mass matrix on the unknowns. The matrix appearing in the second-order term on the right-hand side is recognized as the stiffness matrix. It is the presence of this extra term which accounts for the enhanced phase accuracy and stability of the Taylor–Galerkin scheme over previous finite-element formulations for hyperbolic problems. Equation (5) can be written in the more compact form

$$M_C\,\delta\mathbf{u} = \mathbf{f}, \tag{6}$$

where M_C is the consistent mass matrix and $\delta\mathbf{u}$ and $\mathbf{f}$ are nodal vectors. The matrix M_C can be inverted by a simple iterative technique. Denoting as M_L the lumped mass matrix, we write

$$\delta\mathbf{u}^{k+1} = M_L^{-1}\{\mathbf{f} + (M_L - M_C)\,\delta\mathbf{u}^k\}. \tag{7}$$

It has been found empirically for triangular elements that three iterations suffice. Wathen [21] has recently analyzed upper bounds for the condition number of the assembled mass matrix as derived from element mass matrices. From these he estimates convergence rates for triangular elements that are sufficient to account for this experience.

To apply this method to electromagnetic propagation we merely rewrite Maxwell's equations in a standard hyperbolic form. For example, for vacuum fields in 2D

$$\frac{\partial}{\partial t}\begin{pmatrix} E_x \\ E_y \\ E_z \\ B_x \\ B_y \\ B_z \end{pmatrix} = -\frac{\partial}{\partial x}\begin{pmatrix} 0 \\ cB_z \\ -cB_y \\ 0 \\ -cE_z \\ cE_y \end{pmatrix} - \frac{\partial}{\partial y}\begin{pmatrix} -cB_z \\ 0 \\ cB_x \\ cE_z \\ 0 \\ -cE_x \end{pmatrix}, \tag{8}$$

where now c is the speed of light. We take as our degrees of freedom the x, y, and z components of the fields at the nodes of triangles on an unstructured grid. In practice, rather than implementing the scheme in the form shown by (5), we use an equivalent two-step procedure described elsewhere [19]. This procedure is the finite-element equivalent of the familiar two-step Lax–Wendroff algorithm. We shall refer to it as the Lax–Wendroff Taylor–Galerkin (LWTG) scheme.

To demonstrate the basic accuracy of the Taylor–Galerkin method, we consider the problem of resonant electromagnetic waves in a cylindrical cavity. In Fig. 4 we show an unstructured grid filling a circular region. If the boundary is taken to be a conducting wall, then the interior region will support a series of electromagnetic normal modes whose forms and frequencies are well known [Ref. 22, Chap. 8]. We initialized the electromagnetic fields in transverse-electric (TE) polarization as a mixture of the first eight normal modes for the cavity. These fields were evolved in time using the LWTG scheme. We then Fourier-analyzed the time series from an arbitrary sample point in the interior to obtain the frequencies. Figure 5 shows the resulting spectrum. The cavity mode numbers (m, n) and analytical frequencies ω_{mn} are indicated, where m and n are the azimuthal and radial mode numbers and $\omega_{mn} = x'_{mn}$, the nth zero of the derivative of a Bessel function, $J'_m(x)$. The agreement between the analytical and numerical results is very good.

A careful inspection of the mode amplitudes for the cavity test confirms that the Lax–Wendroff scheme is slightly dissipative. This property may render LWTG inappropriate for certain applications. In such cases, the following second-order leapfrog scheme may be a better option. To derive it, we expand $\mathbf{E}^{n+1}$ and $\mathbf{E}^n$ about $\mathbf{E}^{n+1/2}$,

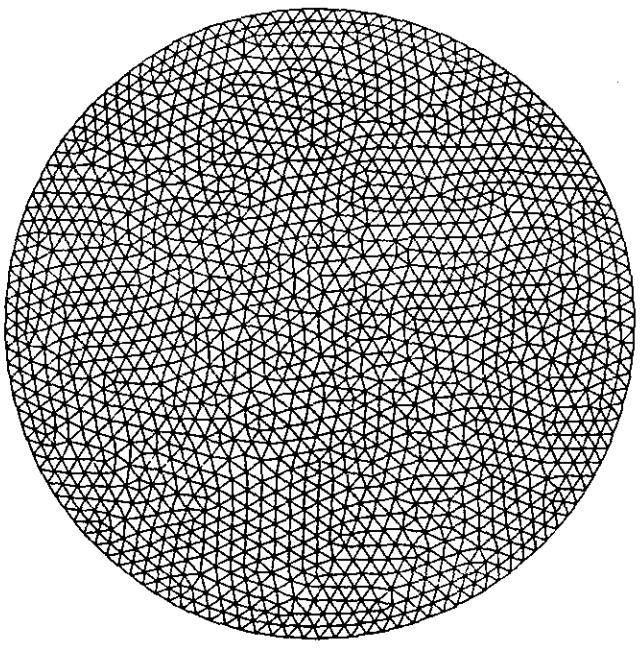

FIG. 4. A quasi-uniform triangulation of the interior of a circular conducting cavity as generated by the advancing front method.

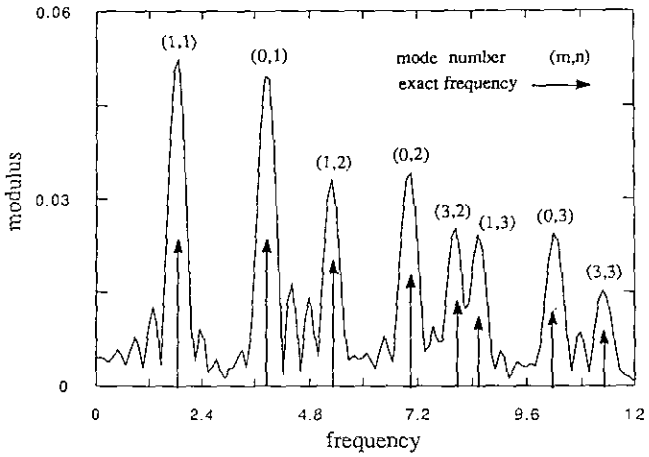

FIG. 5. The power spectrum obtained by Fourier transforming the time series at an arbitrary point within the circular cavity of Fig. 4. The arrows indicate the exact frequencies of eight normal modes that were superimposed to initialize the fields.

$$\mathbf{E}^{n+1} = \mathbf{E}^{n+1/2} + \frac{1}{2}\Delta t \frac{\partial \mathbf{E}^{n+1/2}}{\partial t} + \frac{1}{8}\Delta t^2 \frac{\partial^2 \mathbf{E}^{n+1/2}}{\partial t^2} + O(\Delta t^3), \tag{9}$$

$$\mathbf{E}^{n} = \mathbf{E}^{n+1/2} - \frac{1}{2}\Delta t \frac{\partial \mathbf{E}^{n+1/2}}{\partial t} + \frac{1}{8}\Delta t^2 \frac{\partial^2 \mathbf{E}^{n+1/2}}{\partial t^2} + O(\Delta t^3), \tag{10}$$

and perform similar expansions for $\mathbf{B}^{n+3/2}$ and $\mathbf{B}^{n+1/2}$ about $\mathbf{B}^n$. On subtracting the expansions and substituting expressions for the time derivatives we obtain

$$\mathbf{E}^{n+1} = \mathbf{E}^n + c\,\Delta t\,\nabla \times \mathbf{B}^{n+1/2}, \tag{11}$$

$$\mathbf{B}^{n+3/2} = \mathbf{B}^{n+1/2} - c\,\Delta t\,\nabla \times \mathbf{E}^{n+1}. \tag{12}$$

One then applies the Galerkin approximation to (11) and (12) to complete the derivation of the leapfrog Taylor–Galerkin (LFTG) algorithm.

The advantage of the LFTG scheme is that, although its phase errors are greater, it is dissipation-free. In Fig. 6 we show the time histories of the field energy for a test problem solved with both the LWTG and LFTG formulations. In this problem a perturbation in the B_z component at the center of a square domain produces an outgoing cylindrical wave. The domain was first discretized into square cells and then into triangles by dividing the cells along their

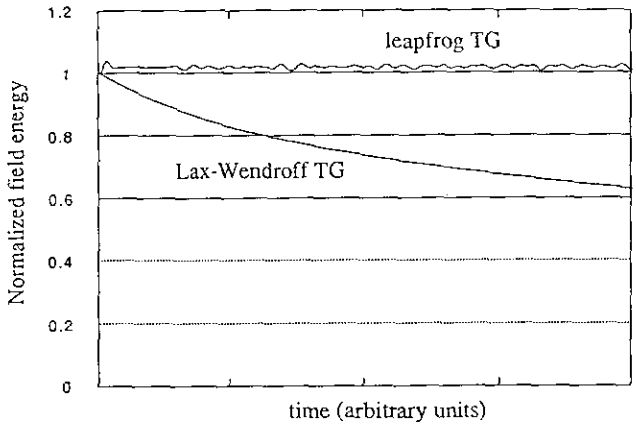

FIG. 6. Time dependence of the field energy in a test case comparing two different Taylor-Galerkin schemes. The Lax-Wendroff-type scheme dissipates some field energy with time, while the leapfrog version does not.

diagonals. This gave us approximately 1800 triangles of equal size h. A wavelength was resolved by about eight nodes. In each case, the Courant number $c\,\Delta t/h = 0.5$. These parameters were deliberately chosen to exaggerate the differences in energy conservation by the two schemes. As claimed, the leapfrog algorithm is energy-conserving.

To further demonstrate the accuracy of the LFTG scheme, we consider the passage of an electromagnetic wave through an array of fine wires. The grid for this problem was presented in Fig. 1, Section 2. The incident wave is a TM-polarized, smooth Gaussian pulse propagating from the left. Figure 7 depicts the solution via LFTG after the wave has encountered the wire. Figure 7a displays contours of E_z while 7b shows us a closeup of the magnetic field vectors

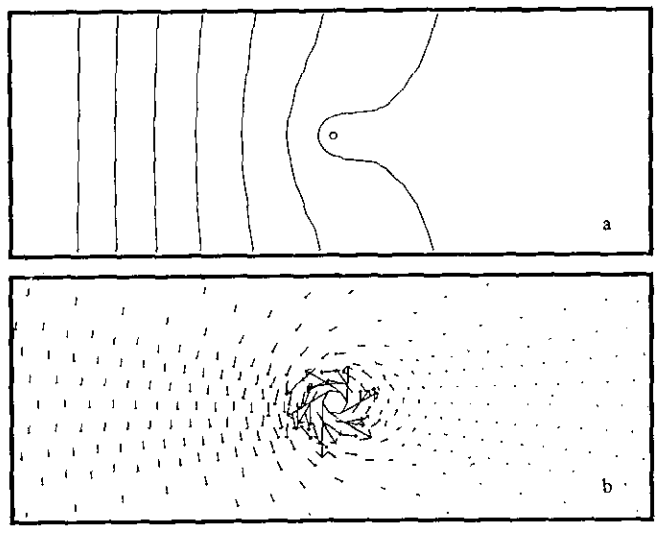

FIG. 7. Results of the a calculation performed in the TM polarization on the grid of Fig. 2. The simulation is periodic in the vertical dimension. A Gaussian pulse propagates past the grid of fine wires: (a) Contours of E_z. (b) A closeup of the magnetic field vectors around the wire.

near the wire. In Fig. 8 we compare a time series from the computed solution, obtained at a time-sample point located halfway down the length of the domain, with the analytic solution. The analytical result is derived from a circuit model of a lossless transmission line in which the wire screen is represented by a shunt impedance [23, 24]. The agreement between the two clearly is excellent.

A special consideration for electromagnetic applications concerns the divergence constraints. In a vacuum, the fields must satisfy $\nabla \cdot \mathbf{B} = \nabla \cdot \mathbf{E} = 0$. Taking the divergence of the Faraday and Ampere laws, one finds that these divergence constraints are satisfied for all time if they are satisfied initially. This follows directly from the continuum property $\nabla \cdot \nabla \times \mathbf{B} = \nabla \cdot \nabla \times \mathbf{E} = 0$. Unfortunately, this may not be true in the discrete approximation. Conventional central finite-difference approximations on staggered meshes possess a special symmetry that causes the discrete divergence of the discrete curl to vanish. Thus, the constraints on the fields are preserved by the time-marching algorithm. In our Taylor–Galerkin schemes, the divergence constraints are not satisfied exactly. However, we believe this is not a serious difficulty for typical computational electromagnetics applications.

All that we require is (a) the divergence-errors to be non-disruptive, i.e., not leading to false solutions, and (b) the divergence errors to vanish with at least the same order as the solution error as the mesh is refined, i.e., a *consistent* reduction of the divergence-errors. This "relaxed" enforcement of the divergence mimics recent developments in finite element methods for the solution of incompressible flow problems [25].

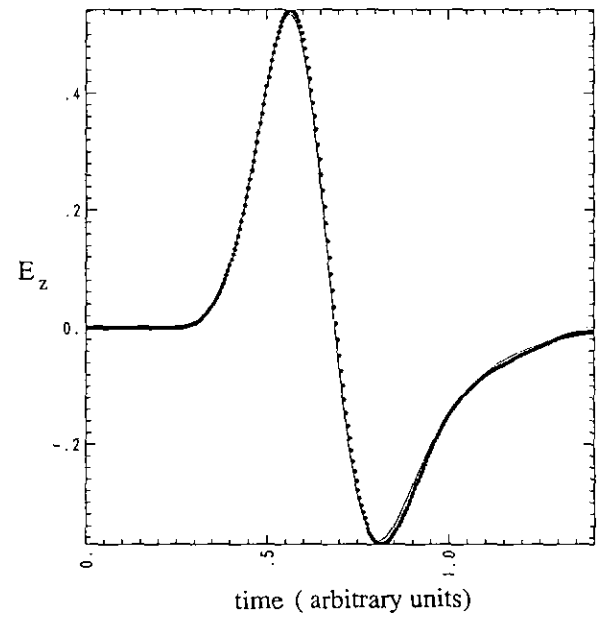

FIG. 8. Comparison of analytic and computed results. The solid curve is the analytical result as obtained from a circuit model. The data points are from the simulation.

Our experience has shown that the divergence errors are small, local, non-accumulating, and consistent with the order of the method. As evidence we present Fig. 9. Here we define the relative error in the divergence of **E** as

$$\varepsilon = \frac{|\nabla \cdot \mathbf{E}|}{|\partial E_x/\partial x| + |\partial E_y/\partial y|}. \tag{13}$$

The discrete form of the divergence in (13) is $\sum_i \nabla N_i \cdot \mathbf{E}_i$. We used the lumped-mass approximation to obtain the nodal values. Similar expressions were used for the terms in the denominator.

An alternative useful measure would be the magnitude of the divergence divided by the magnitude of the curl. For the expansion of a circular wave on a regular square lattice of nodes using LWTG, we present three solutions: one with 20×20 nodes, one with 40×40, and one with 80×80. One can see that the maximum relative error does not accumulate with time. Furthermore, each level of refinement reduces the error by almost an order of magnitude. Thus, we expect accurate answers for any problem that is reasonably zoned. These examples further reinforce the idea that the Taylor–Galerkin procedure and adaptive remeshing are a powerful combination.

An ingenious method of reducing divergence errors following the work of Marder [26] has been tried with some success. Faraday's law can be modified to include a pseudo-current contribution, i.e.,

$$\frac{\partial \mathbf{E}}{\partial t} = c\nabla \times \mathbf{B} + \lambda \nabla(\nabla \cdot \mathbf{E}), \tag{14}$$

where λ is a positive parameter. This contribution has the effect of diffusing the error on the mesh. The method seems to reduce the errors in the interior, but can sometimes pile up errors near boundaries if not handled properly. We found that solutions obtained without the correction were quite accurate when compared against analytical benchmarks.

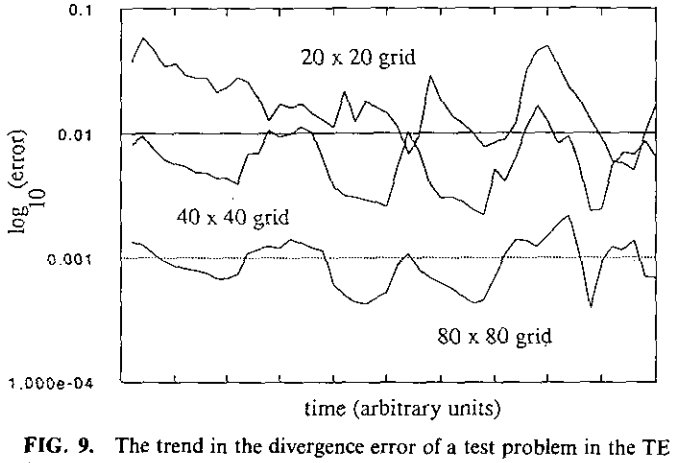

FIG. 9. The trend in the divergence error of a test problem in the TE polarization as a function of zone refinement. Each level of refinement in the zoning reduces the error by almost an order of magnitude, thus confirming the high-order accuracy of the Taylor–Galerkin method.

An enhancement to the basic Taylor–Galerkin algorithm is provided by the addition of a monotone-preserving scheme, such as flux-corrected transport (FCT). FCT was originally developed for hydrodynamic calculations based on finite differences [27, 28]. It has since been extended to finite elements [29] and has been employed successfully in a variety of applications.

The basic idea behind the FCT enhancement is as follows: To prevent the appearance in the final solution of spurious minima and maxima arising from numerical dispersion, a low-order solution $\mathbf{u}^l$ is calculated by replacing M_C by the lumped mass matrix M_L and adding a strong diffusion. The solution obtained by the original algorithm is referred to as the high-order solution $\mathbf{u}^h$. The computed solution is constructed as

$$\mathbf{u}^{n+1} = \mathbf{u}^l + \Delta \mathbf{u}^{\lim}, \tag{15}$$

where at each node

$$\Delta \mathbf{u}^{\lim} = f(\mathbf{u}^h - \mathbf{u}^l), \qquad 0 \leqslant f \leqslant 1, \tag{16}$$

is the largest fraction of the difference between the high-order and low-order solutions that can be applied without creating spurious extrema in $\mathbf{u}^{n+1}$.

The determination of the flux-correction coefficients f in (16) clearly is a critical step in the procedure, establishing as it does the relative mix of the low-order and high-order solutions at each node. We have developed a procedure whereby the coefficients are set by limiting the local excursions of a quadratic form, proportional to the electromagnetic energy density, in all of the variables simultaneously, viz.,

$$Q = |\mathbf{u}^l + f^+ \Delta \mathbf{u}^+ - f^- \Delta \mathbf{u}^-|^2. \tag{17}$$

Here, $\Delta \mathbf{u}^+$ denotes the vector sum of the element contributions $\mathbf{u}^h - \mathbf{u}^l$ having the same sign as $\mathbf{u}^l$ and thus reinforcing it at the given node, and $\Delta \mathbf{u}^-$ as those having the opposite sign. The coefficient f^+ is set to the maximum value which avoids an overshoot in Q for all possible values of f^-, and vice versa. This "synchronization" of the coefficients produces results superior to those obtained by limiting on each of the variables u_j independently, or on a selected single variable of the set.

The allowed local excursions of Q at each node can be determined by checking the values at neighboring nodes only after the low-order changes have been applied (i.e., using $\mathbf{u}^l$ to calculate $Q^{\max}$), or by also looking back to the initial values (using $\mathbf{u}^n$). The former choice tends to "clip" peaked distributions as they propagate across the mesh [28] and thus is somewhat more dissipative, producing smoother field, charge, and current distributions. The latter is more nearly energy-conserving, but tends to generate noisier solutions.

In electromagnetic scattering applications, solutions are

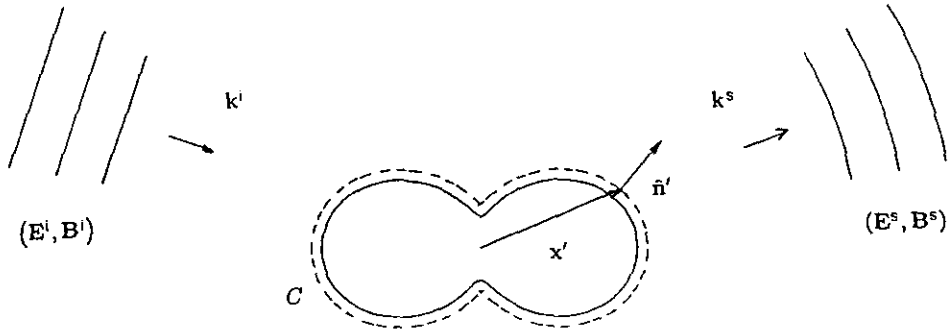

FIG. 10. A schematic representation of the basic scattering problem in electromagnetics. The total electric field at all times is a sum of the incident field E_i and the scattered field E_s.

sought most conveniently by exploiting the linearity of the Maxwell equations and solving for the scattered fields only. The influence of the incident fields is expressed through boundary conditions (at perfectly conducting bodies) and volume source terms (in dielectric and/or permeable media). Away from the scatterer, waves must be outward-propagating. A schematic of this situation is shown in Fig. 10. The FCT enhancement provides an easy and straightforward method for imposing the radiation condition at the outer boundary of the computational domain: the correction coefficients $f^{\pm}$ are set to zero there. The scheme thus becomes essentially upwind at the outer boundary, and the waves are absorbed as they approach the edge of the domain. The slow dissipation of the clipping limiter may in fact be a further asset in scattering problems, since it gently damps the waves as they propagate away from the scatterer toward the absorbing boundary.

As an example of an LWTG-FCT solution to a scattering problem, consider Fig. 11. There we display the electric-field vectors and magnetic-field contours for TE-mode scattering by a circular cylinder. The grid for this problem was shown in Fig. 3, Section 2. A plane wave is incident from the left, and the dimensionless parameter $ka = 10$, where k is the wavenumber of the incident wave and a is the radius of the cylinder. Quasi-cylindrical waves are scattered off of the illuminated side of the cylinder, while nearly plane waves are evident on the shadow side. These latter largely cancel the incident wave, leaving a small residual total field ($\mathbf{E}^i + \mathbf{E}^s$, $\mathbf{B}^i + \mathbf{B}^s$) in the shadow. The damping of the scattered waves as they approach the outer boundary can be seen clearly.

In two dimensions, an analysis of the scattering problem yields an asymptotic expression for the scattered electric field $\mathbf{E}^s$,

$$\mathbf{E}^s \sim \left(\frac{2}{\pi k\rho}\right)^{1/2} e^{ik\rho - i\pi/4}\, \mathbf{S}_2(\psi), \tag{18}$$

where ρ is the distance from the scatterer to the observing point and ψ is the scattering angle. The complex scattering amplitude is the integral

$$\mathbf{S}_2(\psi) = \tfrac{1}{4}\oint_C e^{-i\mathbf{k}^s\cdot\mathbf{x}'} \times [\mathbf{k}^s(\hat{\mathbf{n}}'\cdot\mathbf{E}^s) - \mathbf{k}^s\times(\hat{\mathbf{n}}'\times\mathbf{E}^s) - k^s(\hat{\mathbf{n}}'\times\mathbf{B}^s)]\, dl', \tag{19}$$

where $\mathbf{k}^s$ is the wavenumber of the scattered wave, $|\mathbf{k}^s| = k$, and C is any contour completely enclosing the scatterer with unit normal $\hat{\mathbf{n}}'$. The associated differential scattering cross section per unit length is

$$\sigma_2(\psi) = \lim_{\rho\to\infty} 2\pi\rho \frac{|\mathbf{E}^s|^2}{|\mathbf{E}^i|^2} = \frac{4}{k}\frac{|\mathbf{S}_2(\psi)|^2}{|\mathbf{E}^i|^2}. \tag{20}$$

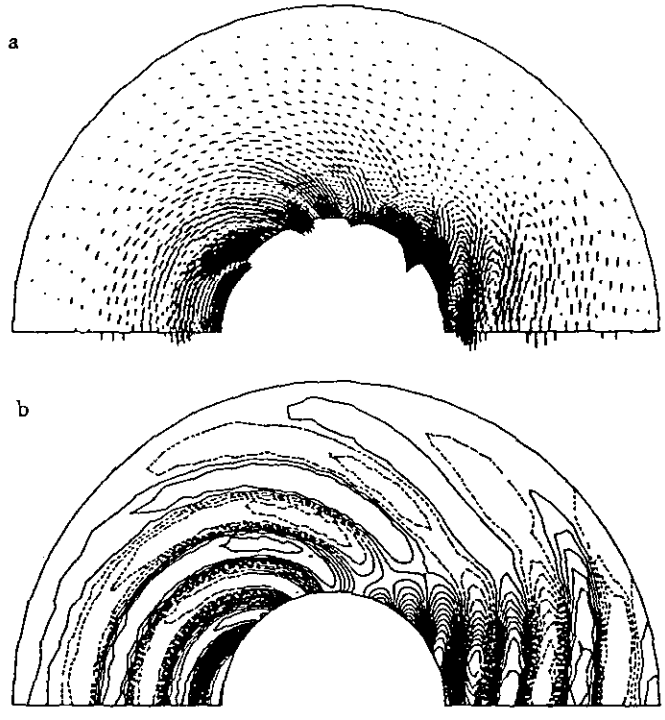

FIG. 11. Final results of the scattering calculation performed on the grid of Fig. 3b: (a) Scattered electric field vectors. (b) Scattered magnetic field contours.

The dependence on the incident wavevector $\mathbf{k}^i$ is implicit in the scattered fields ($\mathbf{E}^s$, $\mathbf{B}^s$). Expressions similar to (18)–(20) hold for the scattering amplitude $S_3(\theta, \phi)$ and differential scattering cross section $\sigma_3(\theta, \phi)$ in three dimensions [Ref. 22, Chap. 9].

We have evaluated the Fourier amplitudes of the scattered fields for the solution shown in Fig. 11 and used them to calculate the scattering amplitude $S_2(\psi)$ for the cylinder. The result is shown in Fig. 12. For comparison, we also show the analytical solution to this problem [30], which was evaluated by machine summation of the series expansions. The agreement is excellent. A broad plateau is evident in the scattering amplitude at angles near back scattering ($\psi \approx 180°$), and a characteristic, modulated diffraction pattern near forward scattering ($\psi \approx 0°$). Note that the amplitude varies with the scattering angle by more than an order of magnitude, corresponding to some 25 dB of variation in the cross section $\sigma_2(\psi)$. All of this structure is reproduced accurately by the numerical solution. The excellent 'agreement observed on the integrated values represented by the Fourier amplitudes corresponds to similarly good agreement in the primitive variable **E** and **B**. Comparable results have been obtained for the complementary, transverse-magnetic (TM) mode of scattering. Empirical comparisons have shown that scattering errors are evidently second-order in the mesh spacing. This was deduced from computations on regular meshes at three different element sizes and two different wavelengths.

The methods proposed in this paper are reasonably fast when properly programmed. The Lax–Wendroff style Taylor–Galerkin method running on a two-processor Cray X-MP took about 15 μs per node per timestep.

4. CONCLUSIONS

Our results demonstrate that the Taylor–Galerkin finite element method is a very useful and powerful technique for solving problems in computational electromagnetics. We have considered two basic formulations. The first, a Lax–Wendroff type scheme, has excellent phase accuracy but is slightly dissipative, the amount of dissipation depending inversely on the Courant number. The second, a leapfrog variant, is non-dissipative but not as accurate in its phase properties. Both methods are, however, at least second-order accurate. Although neither guarantees that divergence constraints are locally satisfied, the errors introduced are small if the problem is properly zoned. For problems involving propagation or scattering, these divergence errors should not be a concern.

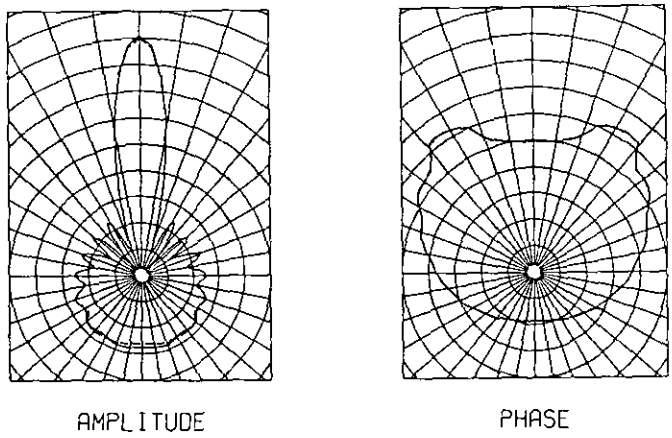

FIG. 12. The scattering amplitude and phase as a function of angle for the problem depicted in Figs. 3 and 11. The solid line is the exact result while the dashed line is computed.

The Lax–Wendroff algorithm can be enhanced by adding a monotone-preserving scheme such as flux-corrected transport. This allows the high-order-accurate LWTG solution to be used wherever the result does not violate the monotonicity constraints imposed by the flux limiter. In other regions, just enough additional dissipation is provided locally to prevent the creation of new extrema. The solutions obtained with the LWTG-FCT scheme are smoother and, for our scattering tests at least, more accurate than those obtained without the FCT enhancement. Thus, LWTG-FCT is generally preferred to the bare LWTG scheme. However, for problems in which the dissipation must be kept to an absolute minimum, the dissipationless LFTG (leapfrog) scheme without FCT then would be the method of choice.

These Taylor–Galerkin schemes implemented on unstructured grids offer a great advantage for electromagnetic problems. They allow small features to be zoned within a large-scale problem with a minimum number of zones. They also allow complicated geometric objects to be realistically and efficiently represented. The flexibility of using unstructured grids permits the mesh to be refined either dynamically, as in the *H*-refinement technique, or iteratively, as in the adaptive-remeshing approach. The powerful combination of the Taylor–Galerkin procedure with unstructured grids could make time-domain electromagnetic calculations the method of choice for an even broader class of applications than is now the case.

Parenthetically, we note that this conclusion may apply equally well in some areas of computational acoustics. There, the Maxwell equations are replaced by the acoustic (linearized hydrodynamical) equations, which have a similar hyperbolic structure. Indeed, it is easy to show that there is a one-to-one mapping between scattering problems involving perfect conductors and TE- or TM-mode electromagnetic waves on the one hand, and acoustic waves striking perfectly hard or soft objects, respectively, on the other.

In electromagnetics, there is one area of application for which Taylor–Galerkin schemes are probably not optimal. These relate to simulations involving charged particles. In particle-in-cell (PIC) simulations of plasmas and beams,

the fundamental requirements of a good field algorithm emphasize different aspects of the solution than those in other areas of computational electromagnetics. In particular, the small relative divergence, or charge-conservation, errors that can be readily tolerated in propagation problems, may produce serious errors in PIC codes. On the other hand, dispersion errors and other numerical pathologies that are potentially deadly to scattering problems are not as serious for PIC. What is important is that the solution algorithm be fast and more or less second-order accurate. Moreover, the solution must be free of divergence (charge-conservation) errors. Recent finite volume methods [31] may be more appropriate for PIC applications.

In conclusion, we believe that the Taylor–Galerkin techniques we have described for electromagnetics on unstructured grids are very powerful and versatile. One of the advantages of the approach is that it is formulated as a hyperbolic problem in which the electromagnetic nature of the problem is expressed solely in terms of its fluxes and boundary conditions. This means that it is possible to combine a number of linear and nonlinear hyperbolic physics models within a unified framework. Thus, such processes as electromagnetic and acoustic scattering, fluid dynamics, heat transport, and others can exist at minimal complexity within the same simulation code. This could be a great advantage in the next generation of general-purpose scientific and engineering software.

ACKNOWLEDGMENTS

We thank Scott Ray and Peter Rambo for contributing their valuable ideas to this project. This work was performed under the auspices of the U.S. Department of Energy by Lawrence Livermore National Laboratory under Contract W-7405-Eng-48, of the Defense Advanced Research Projects Agency through the Applied and Computational Mathematics Program, and of the Office of Naval Research through the Naval Research Laboratory.

REFERENCES

1. K. S. Yee, *IEEE Trans. Antennas. Propagat.* **AP-14**, 302 (1966).
2. A. Taflove and K. R. Umashankar, in *Progress in Electromagnetics Research*, Vol. 2, edited by M. A. Morgan (Elsevier, New York, 1990), p. 287.
3. K. Umashankar and A. Taflove, *IEEE Trans. Electromagn. Compat.* **EMC-24**, 397 (1982).
4. M. E. Jones, "Electromagnetic PIC Codes with Body-Fitted Coordinates," in *12th Conference on the Numerical Simulation of Plasmas, San Francisco, California, Sept. 20–23, 1987.*
5. N. K. Madsen and R. Ziolkowski, *Wave Motion* **10**, 583 (1988).
6. R. L. Lee and N. K. Madsen, *J. Comput. Phys.* **88**, 284 (1990).
7. V. Shankar, W. Hall, and A. H. Mohammadian, in *Proceedings, 9th AIAA Computational Fluid Dynamics Conference, Buffalo, NY, 1989* (American Institute of Aeronautics and Astronautics, New York, 1989), p. 551.
8. M. A. Morgan (Ed.), *Finite Element and Finite Difference Methods in Electromagnetic Scattering* (Elsevier, New York, 1990). Contributions by Taflove and Cangellaris are included, among others.
9. A. C. Cangellaris, C.-C. Lin, and K. K. Mei, *IEEEE Trans. Antennas Propagat.* **AP-35**, 1160 (1987). A time-domain, finite-element method on quadrilateral grids.
10. R. Löhner and J. Ambrosiano, "A Finite Element Solver for the Maxwell Equations", in *Proceedings, GAMNI-SMAI Conference on Numerical Methods for the Maxwell Equations, Paris, France, 1989* (SIAM, Philadelphia, 1991).
11. J. Ambrosiano, S. Brandon, and R. Löhner, "Electromagnetic Propagation on an Unstructured Finite Element Grid", in *Proceedings, 6th Annual Review on Progress in Computational Electromagnetic, Monterey, CA, 1990*, edited by S. Ray (Appl. Comput. Electromagn. Soc., 1990), p. 155.
12. R. Löhner, *Commun. Appl. Numer. Methods* **4**, 123 (1988).
13. R. Löhner and P. Parikh, *Int. J. Numer. Methods Fluids* **8**, 1135 (1988).
14. D. E. Knuth, *The Art of Computer Programming*, Vol. 3 (Addison–Wesley, Reading, MA, 1973).
15. R. Löhner, *Comput. Methods Appl. Mech. Eng.* **61**, 323 (1987).
16. J. Peraire, M. Vahdati, K. Morgan, and O. C. Zienkiewicz, *J. Comput. Phys.* **72**, 499 (1987).
17. R. Löhner, *Comput. Methods Appl. Mech. Eng.* **75**, 195 (1989).
18. J. Donea, L. Quartapelle, and V. Selmin, *J. Comput. Phys.* **70**, 463 (1987).
19. R. Löhner, K. Morgan, and O. C. Zienkiewicz, *Int. J. Numer. Methods Fluids* **4**, 1043 (1984).
20. R. D. Richtmyer and K. W. Morton, *Difference Methods for Initial-Value Problems* (Wiley, New York, 1967), p. 300.
21. A. Wathen, *IMA J. Numer. Anal.* **7**, 449 (1987).
22. J. D. Jackson, *Classical Electrodynamics* (Wiley, New York, 1975).
23. J. R. Wait, *IRE Trans. Microwave Theory Technol.* **MTT-5**, 99 (1957).
24. J. L. Young and J. R. Wait, *IEEE Trans. Microwave Theory Technol.* **37**, 1136 (1989).
25. R. Löhner, "Simple Elements and Linelets for Incompressible Flows," in *The Finite Element Method in the 1990's* edited by E. Oñate, J. Periaux, and A. Samuelsson (Springer-Verlag, New York/Berlin, 1991), p. 419.
26. B. Marder, *J. Comput. Phys.* **68**, 48 (1987).
27. J. P. Boris and D. L. Book, *J. Comput. Phys.* **11**, 38 (1973); D. L. Book, J. P. Boris, and K. Hain, *J. Comput. Phys.* **18**, 248 (1975); J. P. Boris and D. L. Book, *J. Comput. Phys.* **20**, 397 (1976).
28. S. T. Zalesak, *J. Comput. Phys.* **31**, 335 (1979).
29. R. Löhner, K. Morgan, J. Peraire, and M. Vahdati, *Int. J. Numer. Methods Fluids* **7**, 1093 (1987); R. Löhner, K. Morgan, M. Vahdati, J. P. Boris, and D. L. Book, *Commun. Appl. Numer. Methods* **4**, 717 (1988).
30. T. B. A. Senior and P. L. E. Uslenghi, "The Circular Cylinder," in *Electromagnetic and Acoustic Scattering by Simple Shapes*, edited by J. J. Bowman, T. B. A. Senior, and P. L. E. Uslenghi (North Holland, Amsterdam, 1987), p. 92.
31. N. K. Madsen, *J. Comput. Phys.*, submitted.